



PAPER

[View Article Online](#)
[View Journal](#) | [View Issue](#)
Cite this: *Nanoscale*, 2023, **15**, 1661

Ultra-small α -CsPbI₃ perovskite quantum dots with stable, bright and pure red emission for Rec. 2020 display backlights†

 Chuying Wang,^a Wen Meng,^a Yacong Li,^a Guangyong Xu,^a Min Peng,^a
 Shuming Nie ^b and Zhengtao Deng ^{*a}

The synthesis of α -CsPbI₃ perovskite quantum dots (QDs) with pure red emission around 630 nm is in high demand for display backlight application. However, the phase transition of α -CsPbI₃ to yellow non-emitting δ -CsPbI₃ has been proven to be a great challenge for the classic colloidal synthesis route for perovskite QDs in octadecene (ODE). Herein, we report a novel colloidal synthesis route by replacing ODE with lauryl methacrylate (LMA) as the reaction solvent to improve the solubility of precursors, resulting in small sized α -CsPbI₃ QDs with a diameter of only 4.2 nm, which are the smallest red PQDs reported so far. The corresponding CsPbI₃ QD films exhibit a tunable photoluminescence (PL) emission peak in the bright pure red region of 627 to 638 nm. The CsPbI₃ QD polymer composite films with PL emission at 630 nm exhibit a superior photoluminescence quantum yield (PLQY) and photostability to mixed halide CsPbBrI₂ films under intense illumination. Perovskite light emitting diodes (LED) with the color gamut reaching 96% of the Rec. 2020 standard are achieved using these films. This study provides a high-performance pure red fluorescent material with a robust, low-cost, and reproducible colloidal chemistry that will pave the way for the adoption of perovskite QDs in display backlight application.

 Received 1st October 2022,
 Accepted 6th December 2022

DOI: 10.1039/d2nr05456f

rsc.li/nanoscale

Introduction

Colloidal perovskite nanocrystals have attracted significant attention in perovskite light emitting diodes (LED) and display backlights in the past few years owing to their high luminance, narrow emission linewidth and continuously adjustable band gap.^{1–4} Improved performances have been achieved for perovskite LEDs in the green,⁵ deep red⁶ and near-infrared⁷ emission regions.⁸ However, for mixed halide perovskites, poor structural stability and phase segregation caused by defects have limited their application in the bright red emission region (620–640 nm).⁹ Therefore, CsPbI₃ quantum dots (QDs) within a quantum confined regime have been applied to bright red LEDs.^{8,10,11} The challenge of CsPbI₃ QDs is that they usually exhibit emission in the deep-red region (670–690 nm) and

phase instability in the yellow non-emitting phase. To obtain small perovskite QDs, efforts have been made to reduce the size of CsPbX₃ (X = Cl, Br, I) nanocrystals such as varying the ligand composition,¹² adjusting the amount of the oleylamine–HX mixture,¹³ changing the ratio of Pb to X^{10,14} or controlling the nucleation and growth process¹⁵ in the reaction.

However, growth control of the hot injection method is more complex¹⁶ and some methods for CsPbX₃ (X = Cl, Br) can hardly be applied to CsPbI₃ directly.¹² CsPbI₃ nanocrystals suffer from degradation mainly in two aspects. On the one hand, the as-synthesized CsPbI₃ perovskite nanocrystals are extensively purified and isolated from crude solution using polar anti-solvents^{17–24} to separate CsPbI₃ nanocrystals of small size.²⁵ The polar anti-solvent removes surface-bound ligands, resulting in an increase of surface vacant sites and the aggregation of perovskite nanocrystals,^{26–28} and the uniformity of size distribution decreases. This effect will broaden emissions and reduce the color purity²⁹ as well as the PLQY.²⁵ Thus, various surface treatment approaches^{11,30} are used to stabilize CsPbI₃ nanocrystals. On the other hand, phase instability in the yellow non-emitting phase limits their use. Doping methods such as using Yb²⁺ (ref. 31) and Mn²⁺ (ref. 32) are used to stabilize CsPbI₃. Although doping of Mn can stabilize α -CsPbI₃, higher feed ratios of Mn lead to the precipitation of PbI₂,³² precluding the synthesis of Mn²⁺ alloy α -CsPbI₃ QDs

^aCollege of Engineering and Applied Sciences, State Key Laboratory of Analytical Chemistry for Life Science, National Laboratory of Microstructures, Nanjing University, Nanjing, Jiangsu, 210023, P. R. China.
 E-mail: dengz@nju.edu.cn

^bDepartments of Bioengineering, Chemistry, Electrical and Computer Engineering, and Materials Science and Engineering, University of Illinois at Urbana-Champaign, Urbana, IL, 61801, USA

† Electronic supplementary information (ESI) available. See DOI: <https://doi.org/10.1039/d2nr05456f>

with emission in the bright red region (620–640 nm) using the current method.^{10,33}

Recently, Mir *et al.* developed quantum-confined CsPbI₃ perovskite QDs with bright-red emission and a PL emission maximum at 627 nm and a PLQY close to 100% by using zwitterionic lecithin ligands.³⁴ However, the CsPbI₃ perovskite QDs with high PLQYs can only be maintained in solution. The nearly 100% PLQY of CsPbI₃ QDs in the colloidal phase decreased to 68% for lecithin-stabilized QD films and the PL spectra of the QD films were red-shifted. Xie *et al.* developed CsPbI₃ perovskite LEDs with emission at 636 nm by treatment with 3-phenyl-1-propylamine (PPA), tetrabutylammonium iodide (TBAI) and methyl acetate.³⁵ The surface treatment needs large amounts of anti-solvents and small CsPbI₃ QD films with emission <635 nm still need further research. To fabricate QD polymer composite films for down-conversion perovskite LEDs, a purification process is inevitable for the conventional process as shown in Scheme 1. During the purification process, QDs are precipitated without protection of the colloidal solution for transfer to the UV adhesive, leading to a decrease of PLQY and broadening of the peak linewidth.^{25,36} Thus, a precipitation-free method for small CsPbI₃ QD films is also important for down-conversion perovskite LEDs.

Herein, we use lauryl methacrylate (LMA) instead of octadecene (ODE) as the reaction solvent to synthesize ultra-small CsPbI₃ QDs with a diameter of only 4.2 nm through hot injection. LMA has been reported earlier as both a solvent and hydrophobic alkyl monomer for CsPbBr₃ nanocrystal films.³⁷ LMA enables perovskite polymer composite films to be formed without further purification and redispersion. In addition, the solubility of halide-rich precursors containing Mn is improved. The precipitation of PbI₂ caused by higher feed ratios of Mn in the hot-injection reaction is solved as a result. By adjusting the amount of LMA, the emission peak of pristine CsPbI₃ QD solution can be varied from 653 nm to 631 nm. α -CsPbI₃ QDs are synthesized through adopting the feed ratio of Mn/Pb. The emission peaks of the corresponding QD films are adjusted in the bright red region of 638–627 nm. The bright red perovskite QD polymer composite films exhibit superior stability to conventional mixed halide perovskite nanocrystal polymer compo-

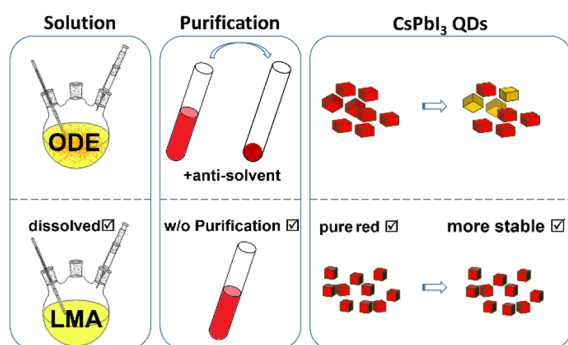
site films. Under continuous intense irradiation, the mixed halide perovskite films undergo phase segregation and the PLQY decreases sharply within 3 hours. In contrast, the PLQY of the CsPbI₃ QD polymer composite film still remains 73% after continuous irradiation for 24 hours. Thus, a down-conversion perovskite LED is fabricated using a green CsPbBr₃ nanocrystal polymer composite film and a bright red CsPbI₃ QD polymer composite film. Moreover, our modified method exhibits a scale-up possibility and reproducibility towards future display applications.

Results and discussion

As for the cubic α -CsPbI₃ phase, the Cs⁺ ions are not large enough to stabilize the cubic framework and a transition to the yellow non-emitting orthorhombic δ -CsPbI₃ phase is seen below 315 °C.³⁸ Mn²⁺ is used to enhance the formation energy and improve the stability of the CsPbX₃ perovskite.^{32,39} However, higher feed ratios of Mn result in the precipitation of PbI₂, which has been reported in a previous work.³² The comparison between CsPbI₃ QD polymer composite films through ODE and LMA strategies are shown in Scheme 1. Compared to ODE, LMA exhibits better solubility for the precursor under the same experimental conditions (Fig. S1†). In the ODE process, the precursor cannot be completely dissolved, and the preparation of the perovskite composite film requires purification using anti-polar solvents to remove the ODE solution. Since the solubility of the precursor affects the halide-rich reaction conditions, Mn-doped CsPbI₃ QDs can hardly reach bright red emission <640 nm through the direct hot-injection method.^{10,33} CsPbI₃ perovskite QDs obtained using ODE exhibit an emission peak at 642 nm (Fig. S2a†). To separate QDs, perovskites need to be purified using methyl acetate. The removal of surface-bound ligands using polar anti-solvents results in the degradation of QDs.^{26–28} Without the protection of the surface ligands, small QDs are easily transferred to the non-emitting δ -CsPbI₃. Furthermore, the CsPbI₃ QDs are not yet stable in pristine ODE solution.

As shown in Fig. 1a, the as-synthesized samples in pristine ODE solution exhibit no significant absorption peaks in the range from 450 nm to 600 nm. After 1 day, a peak around 504 nm appears, indicating that the ODE sample dissociates into monolayer nanocrystals.⁴⁰ After 2 days, an absorption peak located at 517 nm is observed. This peak reflects the formation of monolayer nanoplates³⁶ confirmed by the XRD patterns (Fig. S2b†). Aggregation, phase transition non-emitting phase and self-assembly to the monolayer⁴¹ nanosheets of the samples take place spontaneously after 2 days. The absorption peak at 555 nm appears after the storage of the samples for over 3 days. The peak is attributed to bi-layer nanocrystals.^{36,42} Compared to the ODE samples, the LMA samples exhibit superior stability (Fig. 1b). A monolayer peak appears after storage for over 6 days in the LMA solution (Fig. S3†).

The stability comparison between the samples in ODE and LMA can also be observed from the PL emission, as shown in



Scheme 1 Schematic diagram of the conventional ODE strategy and the new LMA strategy for the fabrication process of the perovskite polymer composite films.

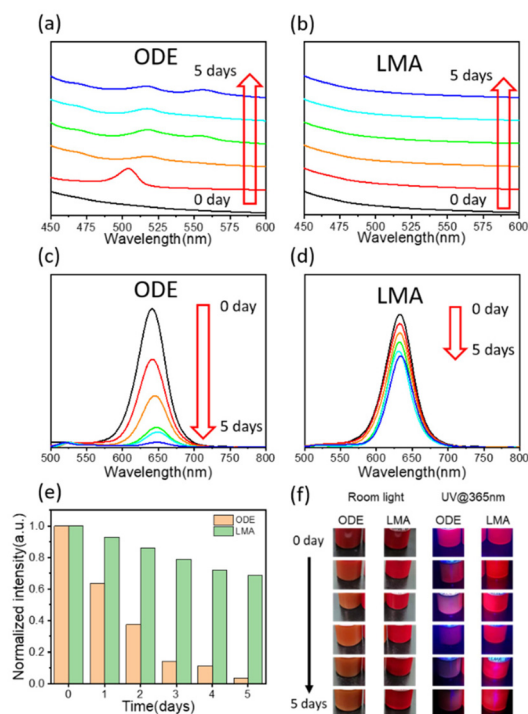


Fig. 1 Comparison of the optical properties between the CsPbI₃ QDs in the ODE and LMA solutions. The absorption spectra of the CsPbI₃ QDs stored in the (a) ODE and (b) LMA solutions for different days without further purification and with a reduced range from 450 nm to 600 nm. The PL emission spectra of the CsPbI₃ QDs stored in (c) ODE and (d) LMA and (e) their comparison in terms of the relative PL intensity. (f) The images of the samples under room light and UV irradiation at 365 nm after storing for different time periods.

Fig. 1c–e. It can be observed that after preservation for 5 days in the pristine solution, the PL intensity of the ODE samples decreases sharply to less than 5%, while the PL intensity of the LMA samples remain at approximately 68% with respect to the initial value. The PL emission peaks of the ODE solution shift from 640 nm to 648 nm after 4 days, while the emission peaks of the LMA samples exhibit nearly no shift until preservation in the solution for 7 days (Fig. S4†). The overall comparison of the optical properties between the two samples is shown directly in Fig. 1f. The degradation of CsPbI₃ QDs is suppressed in LMA and the stability is improved as a result.

LMA provides a preferable environment for Mn-doped CsPbI₃ QDs, which enabled us to conduct more studies on the synthesis of CsPbI₃ QDs. As the high ligand concentration decreases the reactivity of the precursors and nucleus surfaces,⁴³ we can adjust the amount of LMA to increase the concentration of the precursor, according to which the CsPbI₃ QD solution with tunable emission is obtained. As shown in Fig. 2a, with the amount of LMA decreasing from 16 mL to 6 mL, the emission peaks of the QD solution shift from 653 nm to 631 nm. The PL and absorption spectra of CsPbI₃ QDs synthesized using 16 mL of LMA exhibit a red shift compared with those synthesized using 8 mL of LMA after being diluted in toluene (Fig. S5†). As shown in Fig. 2b, the diluted

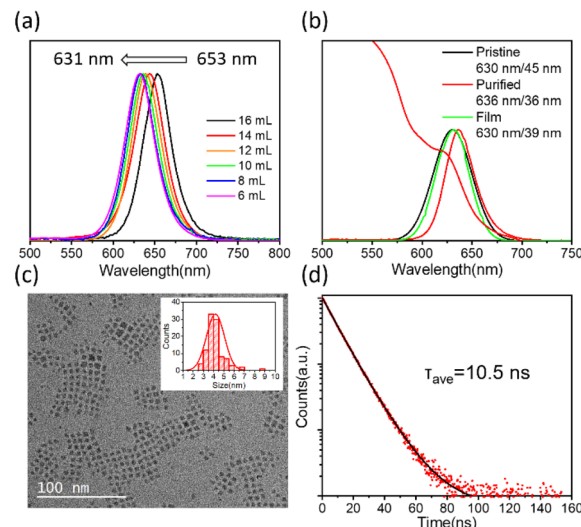


Fig. 2 (a) The PL emission spectra of the QD solution with different amounts of LMA. (b) The PL spectra of the diluted pristine CsPbI₃ QDs, purified QDs and QD films, and the UV-vis absorption spectrum of the purified QDs obtained using 8 mL of LMA, along with their corresponding PL peak wavelength and FWHM. (c) The TEM image of the CsPbI₃ QDs obtained using 8 mL of LMA. The inset shows the size distribution of the CsPbI₃ QDs. (d) The time-resolved PL decay spectrum of the QDs obtained using 8 mL of LMA with Mn/Pb = 1.6.

pristine sample under the condition of 8 mL of LMA exhibits emission at 630 nm with a full width at half maximum (FWHM) of 45 nm. The corresponding QD film exhibits emission at 630 nm with a FWHM of 39 nm, which matches well with the Rec. 2020 standard. After being purified using methyl acetate for once, the PL emission peak shifts to 636 nm with a FWHM of 36 nm, and the absorption is around 620 nm. The CsPbI₃ QDs exhibit a narrower FWHM compared to those in previous works^{11,44} in the bright red region. Purification using polar anti-solvents results in aggregation of small QDs, so a purification-free method for small QD films is also meaningful. The strong quantum confined effect results from the small particles with an average size of 4.2 nm, observed through transmission electron microscopy (TEM) images (Fig. 2c). Compared with the QDs synthesized using 8 mL of LMA, the CsPbI₃ QDs obtained using 16 mL of LMA exhibit a larger mean size of 5.2 nm (Fig. S5†). There is no obvious difference in the Mn/Pb ratio between the QDs synthesized using 8 mL and 16 mL of LMA (Table S1 and Fig. S6†). Thus, the change of the PL peak position is attributed to the variation in QD size controlled through the concentration of precursors. The time-resolved PL (TRPL) decay spectrum is measured and fitted with bi-exponential decay functions as shown in Fig. 2d. The PL lifetimes (τ_{avg}) are listed in Table S2† (with the condition of Mn/Pb = 1.6).

Although doping of Mn²⁺ in CsPbBr₃ and CsPbI₃ cannot be detected through PL emission due to the mismatch between the ⁴T₁ → ⁶A₁ transition of Mn²⁺ and the band gap absorption of the perovskite,^{39,45} Mn²⁺ still has an impact on lead halide perovskites.

The stability of CsPbBr₃ and CsPbI₃ perovskites is influenced by the amount of Mn²⁺.^{32,39} Thus, the feed ratio of Mn/Pb has a crucial effect on the stability of small CsPbI₃ QDs. The improved solubility of the precursor in LMA makes it possible to adjust the feed ratio of Mn/Pb for small QDs. As shown in Fig. 3a, the UV-vis absorption spectra indicate that CsPbI₃ QDs with a feed ratio of Mn/Pb = 1.6 exhibit superior stability after being purified using methyl acetate twice, compared to the undoped CsPbI₃ QDs and QDs with other feed ratios. The QDs with Mn/Pb = 1.6 exhibit an absorption peak at 625 nm. The red shift originates from the removal of surface ligands in the purification process using methyl acetate.²⁵ In addition, QDs with the conditions of Mn/Pb = 1.5 and Mn/Pb = 1.7 exhibit an exciton absorption peak at around 500 nm, which comes from the formation of single layer nanocrystals^{36,46} dissociated from the QDs. QDs with the conditions of Mn/Pb = 0 and Mn/Pb = 1.8 turn into yellow precipitates after the same purification process and lose their luminescence. The PL peaks of the diluted pristine colloidal QD solution with the conditions of Mn/Pb = 1.5, 1.6 and 1.7 all centered at 630 nm (Fig. S7†). After being purified using methyl acetate once, the PL spectra of the QDs with the conditions of Mn/Pb = 1.5 and Mn/Pb = 1.7 show a small peak at 513 nm (Fig. 3b), which originates from the single layer nanocrystals,^{36,46} corresponding to the absorption spectra. The CsPbI₃ QDs with a feed ratio of Mn/Pb = 1.6 exhibit a single emission peak. The PL decay curves and PL decay parameters of QDs with different feed ratios are shown in Fig. 3c and Table S2.† QDs with the conditions of Mn/Pb = 1.5 and Mn/Pb = 1.7 exhibit a triexponential decay. The τ_1 , τ_2 , and τ_3 lifetime components belong to the band-edge recombination, shallow trap-mediated recombina-

tion and trap state, respectively.⁴⁷ When Mn/Pb = 1.6, the triexponential decay curve of the QDs changes to a biexponential decay, and the lifetime component τ_3 corresponding to the trap state disappears. In addition, the phase stability of the QDs is also related to the feed ratio. The samples purified using a large amount of methyl acetate are characterized by XRD, as shown in Fig. 3d. The XRD patterns indicate that CsPbI₃ QDs with Mn/Pb = 1.6 adopt the α -phase perovskite structure.⁴⁸ The samples with a lower feed ratio of Mn/Pb = 1.5 degrade to non-emitting δ -CsPbI₃ and the samples with a higher feed ratio of Mn/Pb = 1.7 degrade to δ -CsPbI₃ and PbI₂, as can be seen in Fig. S8.† With increasing amount of Mn, the stability of CsPbI₃ QDs improves first and then decreases. This phenomenon owes to the change of the formation energy caused by the different amounts of Mn.³⁹ The formation energy will reach the maximum for perovskite after reaching a certain amount of Mn²⁺ content and then decrease rapidly with further increasing content of Mn²⁺. The enhanced formation energy improves the thermal stability and optical performance of the perovskite QDs. As for small CsPbI₃ QDs, the amount of Mn is more critical. As shown in Fig. S9,† QDs with a feed ratio of Mn/Pb > 1.6 are less stable. After being purified using methyl acetate and dried on the Si substrate, the PL emission of QDs with Mn/Pb = 1.7 disappeared and Mn dissociated, while the QDs with Mn/Pb = 1.6 still remained stable. Notably, CsPbI₃ QDs with an appropriate amount of Mn²⁺ exhibit superior stability.

By adjusting the amount of LMA, the emission peaks of the QD solution are tunable, and the emission peaks of the corresponding QD films can be adjusted from 638 nm to 627 nm (Fig. 4a) in the bright red region. The CIE chromaticity coordinates of the red QD films from different amounts of LMA vary continuously from (0.69, 0.31) to (0.67, 0.33), as shown in Fig. S10.† A film with a PL emission peak at 630 nm is achieved under the condition of 8 mL of LMA with a FWHM of 39 nm. As for mixed halide perovskites, phase segregation can be aggravated under photo-illumination.⁴⁹ Phase segregation results in color inhomogeneity and deviation, which limits the reliability of backlight applications.²⁹ Thus, we used CsPbI₃ QD films with bright red emission for backlight applications. CsPbI₃ QD polymer composite films based on LMA are fabricated by photo-polymerization. We compared the optical properties of the bright red emissive films of mixed halide CsPbBrI₂ nanocrystals and CsPbI₃ QDs, as shown in Fig. 4. Triphenylphosphine (TPP)⁵⁰ is used as a stabilizing agent for CsPbBrI₂ films. Fig. S11† shows the cross-sectional images of the CsPbI₃ QD composite film. The thickness of the samples within the two PET substrates is estimated to be ~90 μ m using scanning electron microscopy (SEM) images. The photostability test is executed using a home-made 450 nm LED lamp with irradiance of 1750 mW cm⁻² in a dark room with a distance of 2.5 cm under a relative humidity (RH) of around 70% (Fig. S11d†). As shown in Fig. 4b, the CsPbBrI₂ nanocrystals are unstable in the UV adhesive, leading to a peak blue-shift to 520 nm for the film without TPP. With the protection of TPP, the main peak of the CsPbBrI₂ film shifts from 634 nm to

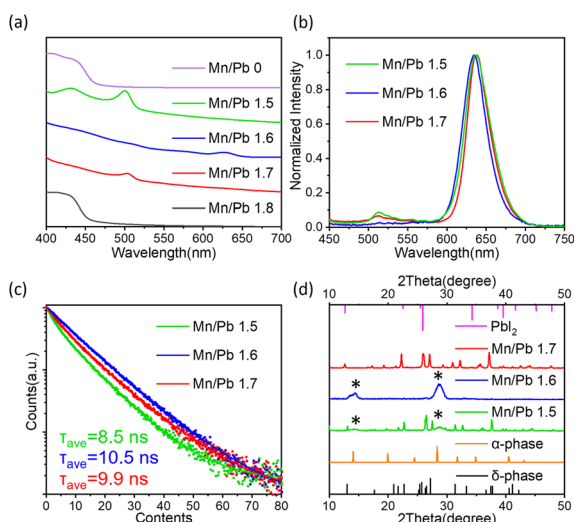


Fig. 3 The influence of the Mn/Pb feed ratio for the CsPbI₃ QDs. (a) The UV-vis absorption spectra of the CsPbI₃ QDs with feed ratios of Mn/Pb = 0, 1.5, 1.6, 1.7 and 1.8. (b) PL emission spectra, (c) time-resolved PL decay spectra and (d) XRD patterns of the CsPbI₃ QDs with feed ratios of Mn/Pb = 1.5, 1.6 and 1.7. The asterisks upon the XRD peaks indicate signals from α -CsPbI₃.

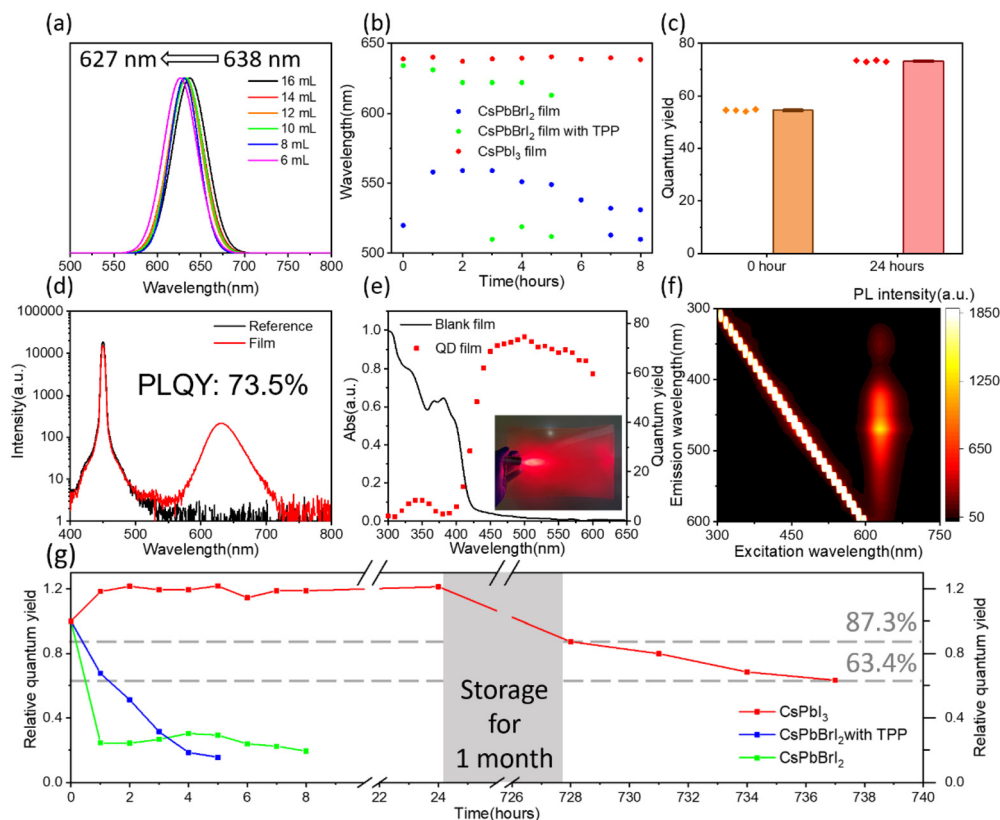


Fig. 4 The PL and stability properties of the perovskite composite films. (a) The PL spectra of the polymer films with CsPbI₃ QDs synthesized using different amounts of LMA. (b) The PL emission peak position of different perovskite polymer composite films under illumination for different time periods. (c) The PLQY of the CsPbI₃ QD films before and after continuous irradiation for 24 h. (d) The PL spectrum of the CsPbI₃ QD film after irradiation for 24 h. (e) The PLQY of the QD films after irradiation for 24 h under various excitation wavelengths (red scatter) and the absorption spectrum of the corresponding blank film (black line). (f) The three-dimensional excitation-emission matrix (EEM) fluorescence spectrum of the CsPbI₃ QD film after irradiation for 24 h. (g) Normalized photostability curves of the perovskite composite films under illumination with respect to the initial PLQY. The inset shows the image of the film.

622 nm, and a second emission peak is detected at 510 nm after 3 h. For the mixed halide perovskites, phase segregation can be aggravated under illumination. The emission peaks of the CsPbI₃ QD films exhibit merely no shift owing to their pure iodide composition.

The time-dependent PLQY characterization of perovskite films is performed as shown in Fig. 4g and Fig. S12.† The main initial emission peak of the CsPbBrI₂ films without TPP was seen to be shifted to 520 nm already, meaning that phase segregation has occurred during the adhesive mixing process. The PLQY of the CsPbBrI₂ films with TPP is 10.3% at the beginning and decreases rapidly under continuous irradiation, reflecting the instability of the mixed halide CsPbBrI₂ perovskite. As for the CsPbI₃ QD films, the PLQY has been improved from 61% to 71% and remain at 73.5% after 24 h. The increase in the PLQY after 1 h owes to the enhanced binding of the carboxylic acid from the ligand in the pristine QD solution.^{37,51} After continuous irradiation, the PLQY and emission peak position of the CsPbI₃ QD films remain stable (Fig. 4b, g and Fig. S11c†). The morphology of the QD films exhibits no obvious change, as shown in Fig. S11b.† When the excitation

wavelength varied from 440 nm to 600 nm, the PLQY of the CsPbI₃ films did not decrease significantly (Fig. 4e) and the peak did not shift (Fig. 4f). As shown in Fig. 4e, the low PLQY with an excitation wavelength <440 nm is generated from the blank film. The change of the PLQY matches well with the absorption spectrum of the blank film. The PLQY of the CsPbI₃ films fabricated using the other UV adhesive did not decrease significantly and the peak did not shift with the variation of the excitation wavelength from 420 nm to 600 nm (Fig. S13†). After 1 month of preservation at room temperature under an average RH over 60%, the PLQY of the CsPbI₃ films decreased to 53% (Fig. S12†), remaining at 87.3% with respect to the initial ratio (Fig. 4g). After continuous intense irradiation for another 9 h, the PLQY decreased to 38%, remaining at 63.4% compared to the initial PLQY. It can be seen that the CsPbI₃ films exhibit superior photostability compared to the mixed halide perovskite film. Therefore, by applying the CsPbI₃ films, the deficiencies that limit the use of lead halide perovskites in LED backlights due to poor structural stability and phase segregation are alleviated in the bright red region.

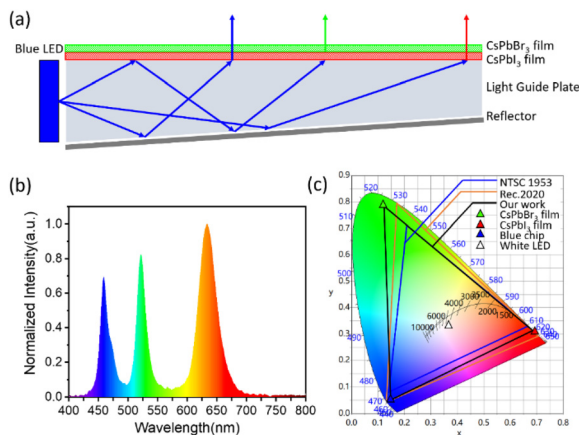


Fig. 5 (a) Schematic illustration of the configuration of the LED backlight. (b) The PL spectrum of a white LED device fabricated from a CsPbBr₃ nanocrystal film and a CsPbI₃ QD film on a 450 nm blue-emitting chip. (c) The color gamut of the LED in the CIE diagram.

The stable CsPbI₃ QD film exhibits emission at 630 nm with a narrow FWHM of 39 nm, which is suitable for display. Thus, a perovskite white LED is fabricated using a CsPbBr₃ nanocrystal polymer composite film and a CsPbI₃ QD polymer composite film. The emission spectra of the blue chip, CsPbBr₃ film and CsPbI₃ film are shown in Fig. S14.† As shown in Fig. 5a, a wide color gamut backlight is fabricated by successively superimposing a CsPbI₃ QD composite film and a CsPbBr₃ composite film on a blue source. The CIE chromaticity coordinates of the blue-chip, green-emissive CsPbBr₃ film and bright red-emissive CsPbI₃ film are (0.15, 0.05), (0.12, 0.79) and (0.69, 0.31), respectively. The CIE chromaticity coordinate of the white point is (0.36, 0.33), with a correlated color temperature (CCT) of 4000 K. The color gamut exceeds 128% of the NTSC1953 standard and 96% of the Rec. 2020 standard in the CIE 1931 color space. Moreover, the synthesis method can be scaled up. As shown in Fig. S15,† the precursor is completely dissolved, and around 250 mL of the colloidal QD solution is collected. The pristine solution exhibits PL emission centred at 630 nm with a FWHM of 44 nm, which is similar to the results shown in Fig. 2b. Thus, our modified method exhibits scale-up possibility and reproducibility towards future display applications.

Conclusions

In summary, we achieved α -CsPbI₃ QD polymer composite films with superior stability in the bright red emission region through a precipitate-free method. By replacing ODE with LMA, the solubility of the precursor has been improved, and thus, a higher feed ratio of Mn for the smallest CsPbI₃ QDs with a diameter of 4.2 nm is achieved so far. The emission peaks of CsPbI₃ colloidal solution change from 653 nm to 631 nm by changing the amount of LMA. The emission peaks of QD films are tunable from 638 nm to 627 nm, with the

corresponding CIE chromaticity coordinates varying from (0.69, 0.31) to (0.67, 0.33). Stable α -CsPbI₃ QDs are obtained through an optimized feed ratio of Mn/Pb. Compared with CsPbBrI₂ composite films, CsPbI₃ QD composite films with emission at 630 nm (FWHM = 39 nm) exhibit superior stability and the peak shift caused by phase segregation is avoided. A white perovskite LED is fabricated using a CsPbBr₃ nanocrystal polymer composite film and a CsPbI₃ QD polymer composite film on a blue light source. An exceedingly wide color gamut of 96% has been achieved through our work relative to the Rec. 2020 standard in the CIE 1931 color space. Our modified method exhibits scale-up possibility and reproducibility towards future display applications. The proposed strategy using LMA paves a new way for effective doping of perovskites and has potential application in high-performance perovskite nanocrystals.

Author contributions

The manuscript was written through contributions of all authors. All authors have given approval to the final version of the manuscript.

Conflicts of interest

There are no conflicts to declare.

Acknowledgements

This work was supported by the National Natural Science Foundation of China (22075129).

References

- 1 Z.-K. Tan, R. S. Moghaddam, M. L. Lai, P. Docampo, R. Higler, F. Deschler, M. Price, A. Sadhanala, L. M. Pazos, D. Credgington, F. Hanusch, T. Bein, H. J. Snaith and R. H. Friend, *Nat. Nanotechnol.*, 2014, **9**, 687–692.
- 2 Q. A. Akkerman, G. Rainò, M. V. Kovalenko and L. Manna, *Nat. Mater.*, 2018, **17**, 394–405.
- 3 X. Shen, Y. Zhang, S. V. Kershaw, T. Li, C. Wang, X. Zhang, W. Wang, D. Li, Y. Wang, M. Lu, L. Zhang, C. Sun, D. Zhao, G. Qin, X. Bai, W. W. Yu and A. L. Rogach, *Nano Lett.*, 2019, **19**, 1552–1559.
- 4 M. V. Kovalenko, L. Protesescu and M. I. Bodnarchuk, *Science*, 2017, **358**, 745–750.
- 5 K. Lin, J. Xing, L. N. Quan, F. P. G. de Arquer, X. Gong, J. Lu, L. Xie, W. Zhao, D. Zhang, C. Yan, W. Li, X. Liu, Y. Lu, J. Kirman, E. H. Sargent, Q. Xiong and Z. Wei, *Nature*, 2018, **562**, 245–248.
- 6 T. Chiba, Y. Hayashi, H. Ebe, K. Hoshi, J. Sato, S. Sato, Y.-J. Pu, S. Ohisa and J. Kido, *Nat. Photonics*, 2018, **12**, 681–687.

- 7 Y. Cao, N. Wang, H. Tian, J. Guo, Y. Wei, H. Chen, Y. Miao, W. Zou, K. Pan, Y. He, H. Cao, Y. Ke, M. Xu, Y. Wang, M. Yang, K. Du, Z. Fu, D. Kong, D. Dai, Y. Jin, G. Li, H. Li, Q. Peng, J. Wang and W. Huang, *Nature*, 2018, **562**, 249–253.
- 8 C. Bi, J. Hu, Z. Yao, Y. Lu, D. Binks, M. Sui and J. Tian, *Adv. Funct. Mater.*, 2020, **30**, 2005990.
- 9 P. Vashishtha and J. E. Halpert, *Chem. Mater.*, 2017, **29**, 5965–5973.
- 10 Y.-K. Wang, F. Yuan, Y. Dong, J.-Y. Li, A. Johnston, B. Chen, M. I. Saidaminov, C. Zhou, X. Zheng, Y. Hou, K. Bertens, H. Ebe, D. Ma, Z. Deng, S. Yuan, R. Chen, L. K. Sagar, J. Liu, J. Fan, P. Li, X. Li, Y. Gao, M.-K. Fung, Z.-H. Lu, O. M. Bakr, L.-S. Liao and E. H. Sargent, *Angew. Chem., Int. Ed.*, 2021, **60**, 16164–16170.
- 11 Y. F. Lan, J. S. Yao, J. N. Yang, Y. H. Song, X. C. Ru, Q. Zhang, L. Z. Feng, T. Chen, K. H. Song and H. B. Yao, *Nano Lett.*, 2021, **21**, 8756–8763.
- 12 A. Dutta, S. K. Dutta, S. Das Adhikari and N. Pradhan, *ACS Energy Lett.*, 2018, **3**, 329–334.
- 13 G. Almeida, L. Goldoni, Q. Akkerman, Z. Dang, A. H. Khan, S. Marras, I. Moreels and L. Manna, *ACS Nano*, 2018, **12**, 1704–1711.
- 14 Y. Dong, T. Qiao, D. Kim, D. Parobek, D. Rossi and D. H. Son, *Nano Lett.*, 2018, **18**, 3716–3722.
- 15 Q. A. Akkerman, T. P. T. Nguyen, S. C. Boehme, F. Montanarella, D. N. Dirin, P. Wechsler, F. Beiglbock, G. Rainò, R. Erni, C. Katan, J. Even and M. V. Kovalenko, *Science*, 2022, **377**, 1406–1412.
- 16 N. Pradhan, *ACS Phys. Chem. Au*, 2022, **2**, 268–276.
- 17 L. Protesescu, S. Yakunin, M. I. Bodnarchuk, F. Krieg, R. Caputo, C. H. Hendon, R. X. Yang, A. Walsh and M. V. Kovalenko, *Nano Lett.*, 2015, **15**, 3692–3696.
- 18 Q. Wang, Z. Jin, D. Chen, D. Bai, H. Bian, J. Sun, G. Zhu, G. Wang and S. Liu, *Adv. Energy Mater.*, 2018, **8**, 1800007.
- 19 J. Kim, B. Koo, W. H. Kim, J. Choi, C. Choi, S. J. Lim, J.-S. Lee, D.-H. Kim, M. J. Ko and Y. Kim, *Nano Energy*, 2019, **66**, 104130.
- 20 J. Kim, S. Cho, F. Dinic, J. Choi, C. Choi, S. M. Jeong, J.-S. Lee, O. Voznyy, M. J. Ko and Y. Kim, *Nano Energy*, 2020, **75**, 104985.
- 21 J. Khan, X. Zhang, J. Yuan, Y. Wang, G. Shi, R. Patterson, J. Shi, X. Ling, L. Hu, T. Wu, S. Dai and W. Ma, *ACS Energy Lett.*, 2020, **5**, 3322–3329.
- 22 J. Xue, R. Wang, L. Chen, S. Nuryyeva, T.-H. Han, T. Huang, S. Tan, J. Zhu, M. Wang, Z.-K. Wang, C. Zhang, J.-W. Lee and Y. Yang, *Adv. Mater.*, 2019, **31**, 1900111.
- 23 A. Chakrabarty, S. Satija, U. Gangwar and S. Sapra, *Chem. Mater.*, 2020, **32**, 721–733.
- 24 S. Cho, J. Kim, S. M. Jeong, M. J. Ko, J.-S. Lee and Y. Kim, *Chem. Mater.*, 2020, **32**, 8808–8818.
- 25 S. Lim, G. Lee, S. Han, J. Kim, S. Yun, J. Lim, Y.-J. Pu, M. J. Ko, T. Park, J. Choi and Y. Kim, *ACS Energy Lett.*, 2021, **6**, 2229–2237.
- 26 Y. Wang, J. Yuan, X. Zhang, X. Ling, B. W. Larson, Q. Zhao, Y. Yang, Y. Shi, J. M. Luther and W. Ma, *Adv. Mater.*, 2020, **32**, 2000449.
- 27 E. Yassitepe, Z. Yang, O. Voznyy, Y. Kim, G. Walters, J. A. Castañeda, P. Kanjanaboos, M. Yuan, X. Gong, F. Fan, J. Pan, S. Hoogland, R. Comin, O. M. Bakr, L. A. Padilha, A. F. Nogueira and E. H. Sargent, *Adv. Funct. Mater.*, 2016, **26**, 8757–8763.
- 28 Y. Kim, E. Yassitepe, O. Voznyy, R. Comin, G. Walters, X. Gong, P. Kanjanaboos, A. F. Nogueira and E. H. Sargent, *ACS Appl. Mater. Interfaces*, 2015, **7**, 25007–25013.
- 29 X. Wang, Z. Bao, Y.-C. Chang and R.-S. Liu, *ACS Energy Lett.*, 2020, **5**, 3374–3396.
- 30 M. Liu, L. Ma, K. Xie, P. Zeng, S. Wei, F. Zhang, C. Li and F. Wang, *J. Phys. Chem. Lett.*, 2022, 1519–1525.
- 31 Z. Dai, J. Chen and B. Yang, *J. Phys. Chem. Lett.*, 2021, 10093–10098.
- 32 Q. A. Akkerman, D. Meggiolaro, Z. Dang, F. De Angelis and L. Manna, *ACS Energy Lett.*, 2017, **2**, 2183–2186.
- 33 H. Ebe, Y.-K. Wang, N. Shinotsuka, Y.-H. Cheng, M. Umano, R. Suzuki, Y. Dong, D. Ma, S. Lee, T. Chiba, E. H. Sargent and J. Kido, *ACS Appl. Mater. Interfaces*, 2022, **14**, 17691–17697.
- 34 W. J. Mir, A. Alamoudi, J. Yin, K. E. Yorov, P. Maity, R. Naphade, B. Shao, J. Wang, M. N. Lintangpradipto, S. Nematulloev, A.-H. Emwas, A. Genovese, O. F. Mohammed and O. M. Bakr, *J. Am. Chem. Soc.*, 2022, **144**, 13302–13310.
- 35 M. Xie, J. Guo, X. Zhang, C. Bi, L. Zhang, Z. Chu, W. Zheng, J. You and J. Tian, *Nano Lett.*, 2022, **22**, 8266–8273.
- 36 C. Otero-Martínez, J. Ye, J. Sung, I. Pastoriza-Santos, J. Pérez-Juste, Z. Xia, A. Rao, R. L. Z. Hoyer and L. Polavarapu, *Adv. Mater.*, 2022, **34**, 2107105.
- 37 J. Tong, J. Wu, W. Shen, Y. Zhang, Y. Liu, T. Zhang, S. Nie and Z. Deng, *ACS Appl. Mater. Interfaces*, 2019, **11**, 9317–9325.
- 38 W. Ahmad, J. Khan, G. Niu and J. Tang, *Sol. RRL*, 2017, **1**, 1700048.
- 39 S. Zou, Y. Liu, J. Li, C. Liu, R. Feng, F. Jiang, Y. Li, J. Song, H. Zeng, M. Hong and X. Chen, *J. Am. Chem. Soc.*, 2017, **139**, 11443–11450.
- 40 Y. Hassan, Y. Song, R. D. Pensack, A. I. Abdelrahman, Y. Kobayashi, M. A. Winnik and G. D. Scholes, *Adv. Mater.*, 2016, **28**, 566–573.
- 41 B. P. Kore and J. M. Gardner, *Mater. Adv.*, 2020, **1**, 2395–2400.
- 42 M. C. Weidman, M. Seitz, S. D. Stranks and W. A. Tisdale, *ACS Nano*, 2016, **10**, 7830–7839.
- 43 J. C. Sadighian and C. Y. Wong, *J. Phys. Chem. C*, 2021, **125**, 20772–20782.
- 44 L. Yang, Y. Zhang, J. Ma, P. Chen, Y. Yu and M. Shao, *ACS Energy Lett.*, 2021, **6**, 2386–2394.
- 45 W. Liu, Q. Lin, H. Li, K. Wu, I. Robel, J. M. Pietryga and V. I. Klimov, *J. Am. Chem. Soc.*, 2016, **138**, 14954–14961.
- 46 C. Wang, Y.-K. Wang, Z. Li, J. Luo, R. Sabatini, T. Zhang, E. H. Sargent and Z. Deng, *Adv. Opt. Mater.*, 2022, **10**, 2200217.
- 47 V. G. V. Dutt, S. Akhil, R. Singh, M. Palabathuni and N. Mishra, *J. Phys. Chem. C*, 2022, **126**, 9502–9508.

- 48 A. Marronnier, G. Roma, S. Boyer-Richard, L. Pedesseau, J.-M. Jancu, Y. Bonnassieux, C. Katan, C. C. Stoumpos, M. G. Kanatzidis and J. Even, *ACS Nano*, 2018, **12**, 3477–3486.
- 49 E. T. Hoke, D. J. Slotcavage, E. R. Dohner, A. R. Bowring, H. I. Karunadasa and M. D. McGehee, *Chem. Sci.*, 2015, **6**, 613–617.
- 50 J. Wu, J. Tong, Y. Gao, A. Wang, T. Zhang, H. Tan, S. Nie and Z. Deng, *Angew. Chem., Int. Ed.*, 2020, **59**, 7738–7742.
- 51 J. De Roo, M. Ibáñez, P. Geiregat, G. Nedelcu, W. Walravens, J. Maes, J. C. Martins, I. Van Driessche, M. V. Kovalenko and Z. Hens, *ACS Nano*, 2016, **10**, 2071–2081.